Lecture 9

Bounds on Mixing in Stratified Shear Flows

Colm-cille P. Caulfield

Notes by Jennifer Siggers

1 Introduction and Motivation

Mixing is a very common feature in the environmentally prevalent flows with both vertical velocity and density variation. Examples include the thermocline, the lutocline, planetary boundary layers, river mouths, etc. Such flows exhibit a characteristic life-cycle, where some external forcing intensifies the velocity shear, triggering a sequence of instabilities. These instabilities typically lead to a period of small-scale disordered turbulent motion, that is characterized by substantially enhanced mixing of fluid elements, and also dissipation. This dissipation inevitably extracts energy from the mean shear, which decreases in magnitude, leading ultimately to relaminarization of the underlying flow. Subsequent external forcing starts the cycle once again.

The problem is that crucial aspects of the life cycle are associated with motions that are inherently small scale, (of the order of millimetres) over time scales that are also short (of the order of seconds), but we wish to know what happens on much larger length and time scales, for example synoptic (i.e. of the order of hundreds to thousands of kilometres) and seasonal scales. For example we may want to know about the total global or atmospheric heat budget or pollutant transport within the entire system. Thus we might want to ask the deceptively simple question:

> For a given kinetic energy input from the shear forcing, how much energy is lost to viscous dissipation and how much energy leads to mixing?

The objective of a significant amount of recent research has been to answer this question by identifying the mixing mechanisms. This has been done by finding the dependence of mixing events on bulk flow characteristics, their spatial localizations and their time dependence. Then it is possible to quantify the mixing appropriately, for example by distinguishing between reversible and irreversible processes and, more recently, by developing rigorous bounds. The ultimate aim that should always be remembered is the desire to generate robust parameterizations, useful to models of larger scale geophysical flows, that capture the essential characteristics of mixing within stratified sheared flow.

2 Energetics of Stratified Shear Flows

To identify some of the important aspects of the energetics of stratified shear flows, consider a simple flow that is infinite or periodic in the horizontal directions and has finite extent in the vertical direction. We use stress free boundary conditions with no normal flow through the boundary and assume an insulating temperature boundary condition. The velocity is assumed to vary from $-U_0$ to $+U_0$ over the length scale d_0, and the density varies from $\rho_a - \rho_0$ to $\rho_a + \rho_0$ over the length scale δ_0, where $\rho_0 \ll \rho_a$. Alternatively,

$N^2(z) = -g/\rho_a \partial\bar{\rho}/\partial z$ where the variation in ρ is "small" over the scale d_0. We therefore assume that the Boussinesq approximation is valid.

Richardson numbers are a useful tool for parameterizing mixing processes. There is a broad class of such numbers. Here, we define two of these; the **bulk Richardson number**:

$$J = \frac{g\rho_0 d_0}{\rho_a U_0^2}, \tag{1}$$

and the **gradient Richardson number**:

$$Ri(z) = \frac{-gd\bar{\rho}/dz}{\rho_a \left(d\bar{u}/dz\right)^2} = \frac{N^2}{(d\bar{u}/dz)^2}, \tag{2}$$

where the bar denotes averaging over the horizontal layer. Both the global (J) and local (Ri) Richardson numbers are a measure of the relative importance of buoyancy force to inertia or alternatively the potential energy variations to kinetic energy variations.

In the Boussinesq approximation, the kinetic energy density of the flow is given by

$$\mathcal{K}(t) = \frac{\langle |\mathbf{u}|^2 \rangle}{2}, \tag{3}$$

where the angle brackets denote the average over the whole layer. We non-dimensionalize the equations with the scales d_0, U_0 and ρ_0. Dotting the Navier–Stokes equation with $\mathbf{u}$ and averaging over the domain yields the evolution equation for $\mathcal{K}$

$$\frac{d\mathcal{K}}{dt} = -J\langle \rho w \rangle - \frac{1}{Re}\langle (\nabla \mathbf{u})^2 \rangle \tag{4}$$

$$\equiv \mathcal{H} - \mathcal{E} = -\mathcal{B} - \mathcal{E}, \tag{5}$$

where $\mathcal{H}$ is the heat flux, $\mathcal{B} = -\mathcal{H}$ is the buoyancy flux and $\mathcal{E}$ is the rate of dissipation.

The potential energy density is defined to be

$$\mathcal{P} = J\langle \rho z \rangle = J\langle \bar{\rho} z \rangle_z, \tag{6}$$

where the subscript z indicates averaging over the z-component only. The evolution equation for $\mathcal{P}$ is

$$\frac{d\mathcal{P}}{dt} = \mathcal{B} + \mathcal{D}_{\mathcal{P}}, \tag{7}$$

where

$$D_{\mathcal{P}} = \frac{2J}{\sigma Re L_z}, \tag{8}$$

and $\mathcal{D}_{\mathcal{P}}$ is the inevtiable diffusion of the mean profile, which would occur in the absence of macroscopic fluid motion.

If the flow is statically stable $\mathcal{D}_{\mathcal{P}} > 0$, denoting a continual conversion of internal energy into potential energy within the Boussinesq approximation. Energy is exchanged between $\mathcal{K}$ and $\mathcal{P}$ via $\mathcal{B}$, see figure 2. Clearly, the buoyancy flux is intimately related to the process of mixing, but it is necessary to have a very clear view of what exactly we mean by mixing before quantitative advances can be made.

3 Concepts of Stirring and Mixing

We consider mixing to be an irreversible change of the fluid properties that is inherently small scale. We wish to distinguish mixing from stirring, which we consider to be a large scale reversible motion of the fluid. Mixing, in our view, corresponds to an irreversible change of $\mathcal{P}$ caused by the motion of the fluid. However, the buoyancy flux $\mathcal{B}$ includes both mixing and stirring, so in order to quantify the amount of mixing taking place, we split the potential energy into two parts, the background potential energy, that is increased irreversibly by the mixing process and the available potential energy that may be reconverted back to kinetic energy, following the original conception of Lorenz. A particular algorithmic formulation, well-suited to numerical simulation was invented in [1], where the background potential energy is defined as

$$\mathcal{P}_B = J\langle \rho_B(z) z\rangle_z, \tag{9}$$

where ρ_B is the background density profile. The background density profile is the sorted statically stable profile of the fluid that has no horizontal variation, and is generated by adiabatic (within our Boussinesq incompressible framework this corresponds to volume-preserving) rearrangement or sorting of the fluid parcels into a state corresponding to the minimum possible potential energy that can be achieved by the flow. An example of the way this sorting is done is shown in figure 1. The remainder of $\mathcal{P}$ is the available potential energy $\mathcal{P}_A$ (i.e. available for reconversion into other forms of energy). We have,

$$\begin{aligned}
\mathcal{P}_A &= \mathcal{P} - \mathcal{P}_B, && (10)\\
\frac{d}{dt}\mathcal{P}_{\mathcal{A}} &= \mathcal{B} - \mathcal{M} = \mathcal{S}, && (11)\\
\frac{d}{dt}\mathcal{P}_{\mathcal{B}} &= \mathcal{M} + \mathcal{D}_{\mathcal{P}}, && (12)\\
\frac{d}{dt}\mathcal{K}(t) &= -\mathcal{S} - \mathcal{M} + \mathcal{D}, && (13)
\end{aligned}$$

where $\mathcal{S}$ and $\mathcal{M}$ are energy transfer rates defined by the above equations. A schematic view of the processes of energy transfer represented by these equations is shown in figure 2. Figure 3 shows a schematic graph of possible values of $\mathcal{B}$, $\mathcal{M}$ and $d\mathcal{P}_A/dt$ for a typical fluid. The left hand half shows a situation where the fluid is moving upwards on average ($\mathcal{B} > 0$). The mixing rate $\mathcal{M}$ can actually be small during this stage, for example during the initial preturbulence roll-up of a Kelvin–Helmholtz billow. In the right hand half, the fluid is moving downwards on average ($\mathcal{B} < 0$), and this can correspond to a higher mixing rate. However, the averages of $\mathcal{B}$ and $\mathcal{M}$ for sufficiently long times are always equal, so that

$$\lim_{t\to\infty}\int_0^t \mathcal{B}dt = \lim_{t\to\infty}\int_0^t \mathcal{M}dt, \quad \text{i.e. } \lim_{t\to\infty}\int_0^t \mathcal{S}dt = 0. \tag{14}$$

4 Mixing Efficiency

Essentially the fundamental question posed in the introduction considers the **efficiency** of the mixing, i.e. the proportion of the kinetic energy lsot by the flow (or the driving

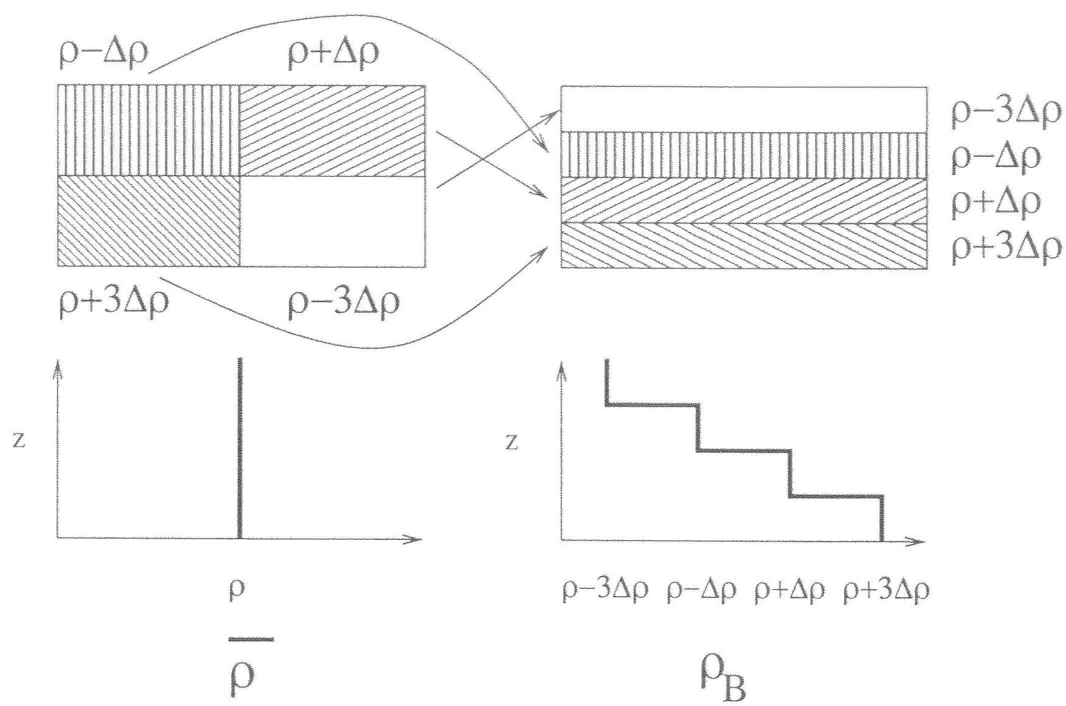

Figure 1: Diagrams showing an example of the actual state of the fluid (top left). The horizontally averaged density $\bar{\rho}$ is shown underneath, which is uniform in z in this case. The sorted stable profile of the fluid for calculating the background density is shown (top right), with the heaviest fluid at the bottom, and the graph of background density is shown underneath.

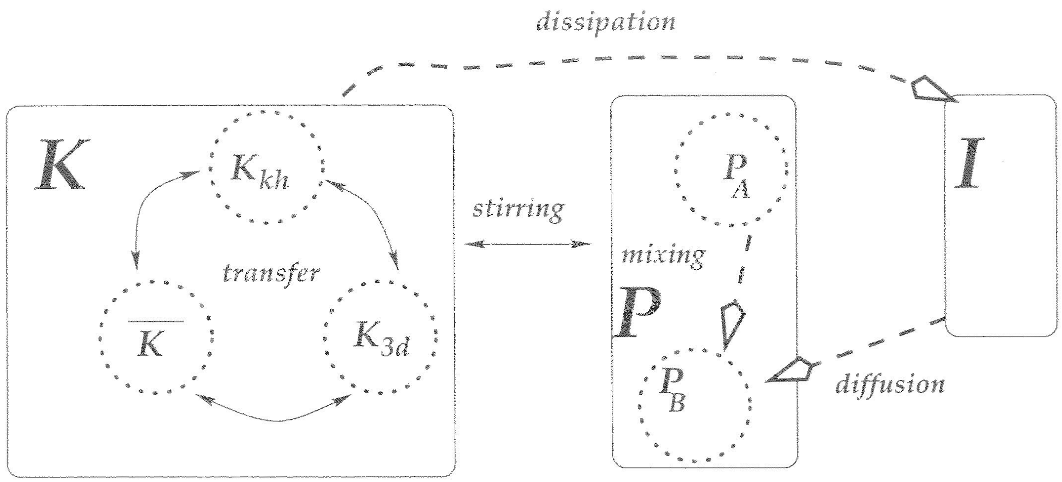

Figure 2: Diagram showing the mechanisms by which energy may be transferred in the fluid. $\mathcal{K}$ is the kinetic energy, $\mathcal{P}$ is the potential energy and $\mathcal{I}$ is the internal energy of the fluid (e.g. due to its temperature).

mechanism) that leads to mixing, or, equivalently, irreversible increases in potential energy. More formally, the mixing efficiency is usually (e.g. for grid–stirred experiments) defined as

$$\frac{\Delta PE}{WORK} \tag{15}$$

(see [2, 3] etc.). This is the natural measure of the proportion of the kinetic energy input to the fluid that has led to irreversible mixing. Experimentally this is typically only determined at the very end of an experiment, once all reversible processes can be assumed to have died out. However, provided the background density profile can be determined explicitly, (as can be done straightforwardly in a numerical simulation) it is possible to define an instantaneous mixing efficiency:

$$\mathcal{E}_i \equiv \frac{\mathcal{M}}{\mathcal{M}+\mathcal{E}}. \tag{16}$$

Naturally, it is also possible to define a long-time cumulative version

$$\mathcal{E}_c \equiv \frac{\int_0^t \mathcal{M}(u)\,\mathrm{d}u}{\int_0^t \mathcal{M}(u)\,\mathrm{d}u + \int_0^t \mathcal{E}(u)\,\mathrm{d}u}, \tag{17}$$

that more closely approximates the experimental quantity.

The beautiful work of Winters [4] has shown that the diapycnal flux Φ_d is

$$\Phi_d = \mathcal{M} + \mathcal{D}_{\mathcal{P}} = -\frac{J}{RePr}\left\langle \frac{dz_*}{d\rho}|\nabla\rho|^2 \right\rangle, \tag{18}$$

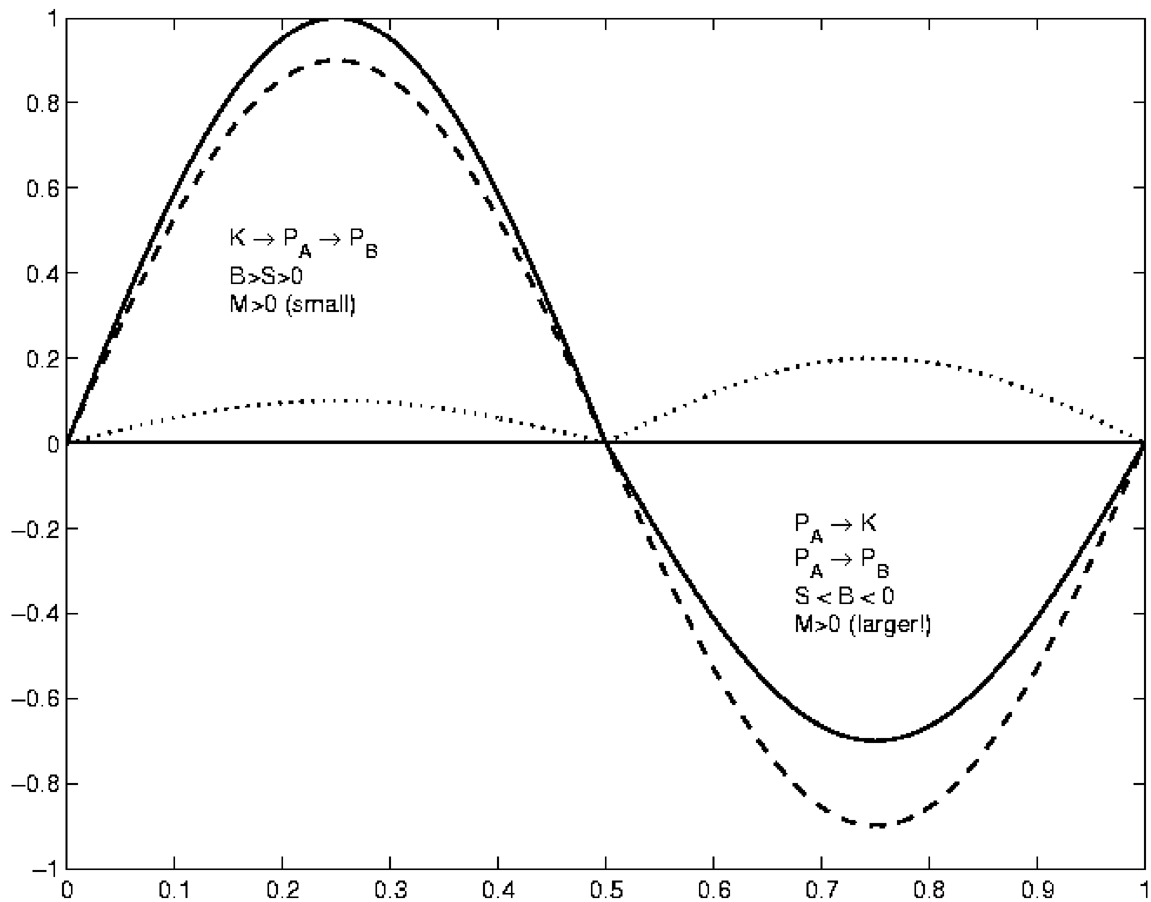

Figure 3: Diagram showing possible values of $\mathcal{B}$ (solid), $\mathcal{M}$ (dotted) and $d\mathcal{P}_A/dt$ (dashed) for a typical fluid as over a period of time.

where z_* is the coordinate associated with the rearanged fluid parcels that make up the background density profile ρ_B. A large Φ_d means that there is an enhanced irreversible transport of density, and hence an irreversible increase in potential energy. From the formula, it is apparent that this may occur if there is an enhanced density gradient and/or enhanced surface area of contact between fluids of different densities. Φ_d can also be related to the Cox number, or equivalently to the flux Richardson number.

The flux Richardson number is defined in sheared stratified turbulent flow as

$$R_f = \frac{\mathcal{B}}{-\langle u'w'\rangle d\bar{u}/dz}, \tag{19}$$

where $\mathbf{u}' = \mathbf{u} - \bar{\mathbf{u}}$. The long time average of R_f always tends to the mixing efficiency $\mathcal{E}_c$. However, the denominator (essentially the shear production of turbulent kinetic energy, which corresponds to the kinetic energy lost by the mean, forcing flow) of the expression for R_f is always positive in a steady state and so if $\mathcal{B} < 0$, which often happens in the periods of most intense mixing then R_f is negative! Hence it does not necessarily provide a good instantaneous estimate of the mixing efficiency.

5 Previous Parameterizations

Previous parametrizations of mixing within shear driven turbulence have focussed on appropriate descriptions of the flux Richardson number, since it is apparent that in a shear flow

$$\frac{R_f}{Ri} = \frac{k_h}{k_m}, \tag{20}$$

where

$$k_h = \frac{\mathcal{B}}{N^2} \quad \text{and} \quad k_m = \frac{-\langle u'w'\rangle}{d\bar{u}/dz}, \tag{21}$$

are the eddy diffusivities of density and momentum respectively. Larger scale models often rely on sub-grid scale parameterizations based on eddy diffusivities. Although such models have many problems, they are commonly used, and so the determination of the flux Richardson number in terms of bulk properties of the flow has been the focus of much research.

For example, the Osborn–Cox Model [5] is a common oceanographic model that assumes that the flow is stationary and homogeneous. Also, both boundary effects and the effects of advection into and out of the domain are assumed to be unimportant. With these assumptions,

$$k_h = \frac{R_f}{1 - R_f}\frac{\mathcal{E}}{N^2} = \Gamma\frac{\mathcal{E}}{N^2}, \tag{22}$$

where Γ is known as the flux coefficient. Historically, often $R_f \approx 0.15$ has been assumed, corresponding to $\Gamma \approx 0.2$ (based on oceanographic observations), although $0.05 \leq R_f \leq 0.3$ have been observed [6, 7]. Rod-stirring experiments suggest $R_f \leq 0.8$ [3] and collated

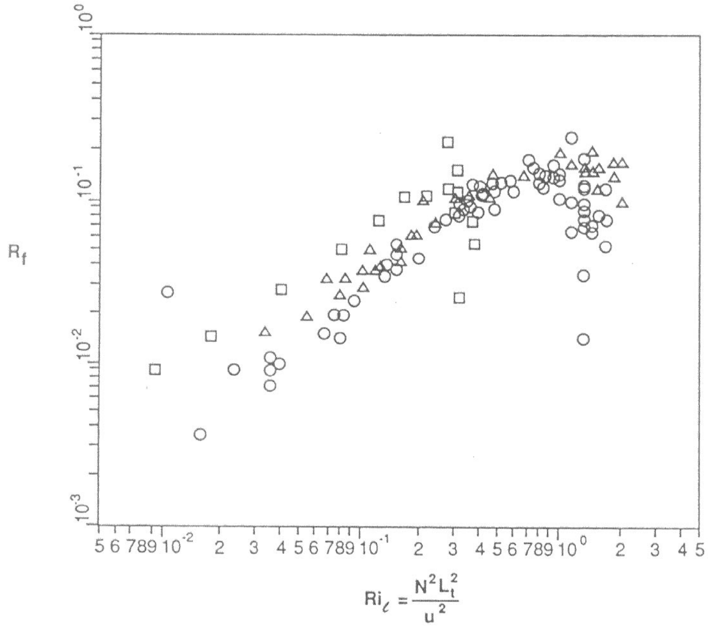

(a)

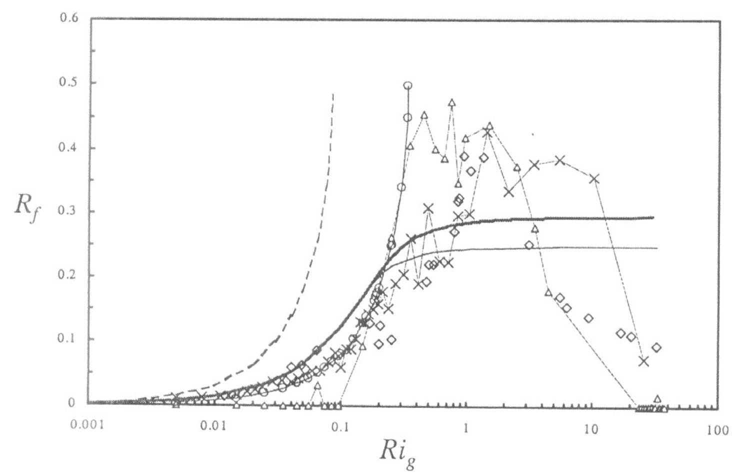

(b)

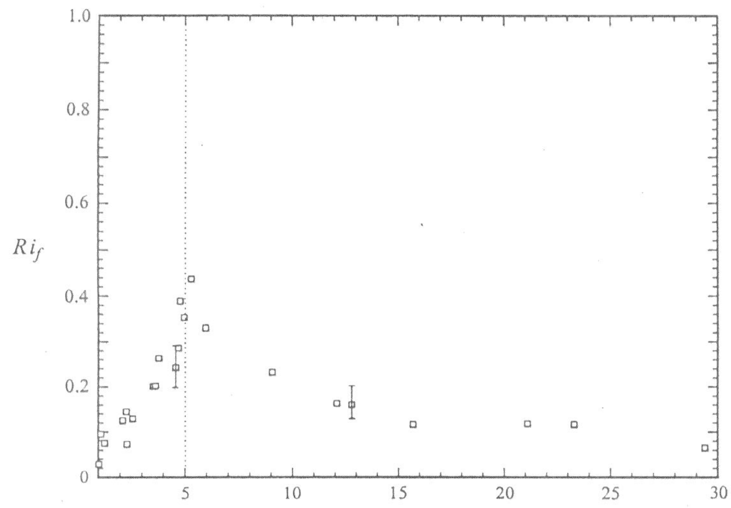

(c)

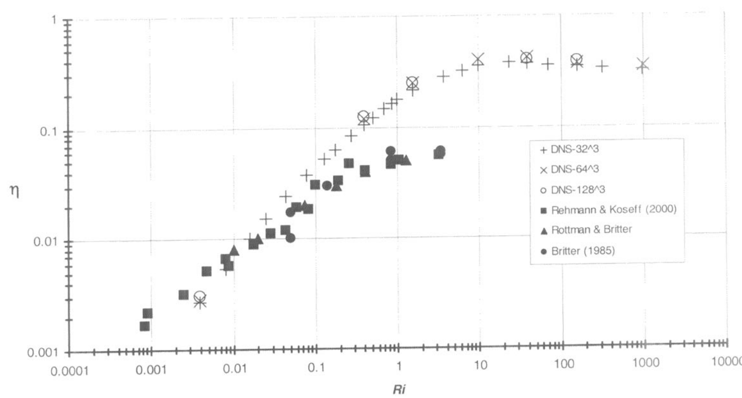

(d)

Figure 4: Four graphs showing values of the flux Richardson number R_f as a function of gradient Richardson number Ri obtained by different sources. (a) Some experimentally measured values. The squares represent thermally stratified wind-tunnel data from [11], and the circles and triangles represent decaying and growing (shear-driven) stratified turbulence data in salinity-stratified fluids, as compiled in [12]. (b) Observed mixing efficiencies. The dashed curve is from [13], the thin solid curve is from [14], the bold solid curve is from [15], the triangles are from an experiment based in Salt Lake City and the crosses are from an experiment based at Los Alamos [16], the diamonds are from [17] and the circles are from a modified version of [13]. The graph is taken from [16]. (c) Experimental values from [17]. (d) Values obtained by direct numerical simulation compared with experimental values (solid symbols).

experiments suggest $R_f \leq 0.2$ [8]. The dependence of the mixing efficiency on Ri and J was found in [9, 10] where is was also found that there is a tendency for the flows to form layers. A graph showing the relationship between Ri and R_f is shown in figure 4(a).

However, some numerical calculations suggest the possibility of larger $\mathcal{E}_c$, and hence R_f, for example in pre-turbulent billows [18, 19, 20]. Also recent direct numerical simulations of homogeneous decaying turbulence suggest $R_f \approx 0.4$, which is consistent with rapid distortion theory calculations at high J [21]. Stratified shear experiments have $R_f \approx 0.45$ and obesrvations have found values of R_f between 0.4 and 0.45 [22, 17, 16]. The graphs in figure 4(b), (c) and (d) show some results that have obtained higher values of R_f.

Some models have also produced high mixing efficiencies. For example, Pearson, Puttock & Hunt [23] found that the mixing was related to local density perturbations and its efficiency was constant (and independent of stratification). There was also an apparent equipartition of $\mathcal{P}$ and $\mathcal{K}$. Weinstock [24] assumed that the dominant mixing processes occur at scales within the inertial subrange (i.e. those scales where there is homogeneous isotropic turbulence, that are much smaller than any characteristic forcing lengthscales and yet longer than the viscous Kolmogorov dissipation lengthscale). He showed, by manipulation of the Lagrangian velocity correlation function that k_h is predicted to take a value consistent with $R_f = 4/9$.

6 Townsend's Model

Townsend [25] developed an empirical model for the heat and momentum transport in turbulent stratified flow. His fundamental assumption was that the turbulence is little affected by the stratification of the fluid. This is obviously not the case in flows where the turbulence is driven on sufficiently large vertical length scales, for which the turbulent motions in the vertical direction are likely to be hindered by the stratification. However, if the dominant turbulent scales have sufficiently small scales, the turbulence can be assumed to be relatively independent of the stratification.

Townsend's empirical assumption is that all flow quantities can be described by characteristic scales of u and the density fluctuations ρ. We define the r.m.s. turbulent kinetic energy intensity q

$$q = \sqrt{\overline{|\mathbf{u} - \overline{\mathbf{u}}|^2}}, \tag{23}$$

and the r.m.s. density fluctuations r,

$$r = \sqrt{\overline{|\rho - \overline{\rho}|^2}}. \tag{24}$$

The equations for the flow $\mathbf{v}$ and the density fluctuations ρ in the Boussinesq approximation are

$$\frac{\partial \mathbf{u}}{\partial t} + \mathbf{u} \cdot \nabla \mathbf{u} + \nabla p = -\rho \frac{\mathbf{g}}{\overline{\rho}} + \nu \nabla^2 \mathbf{u}, \tag{25}$$

$$\frac{\partial \rho}{\partial t} + \mathbf{u} \cdot \nabla \rho = \kappa \nabla^2 \rho, \tag{26}$$

$$\nabla \cdot \mathbf{u} = 0. \tag{27}$$

Assuming that the dominant flow is horizontal, the flow field can be written as

$$\mathbf{u} = U(z)\mathbf{x} + \mathbf{v}(\mathbf{r}) \text{ where } U(z)\mathbf{x} = \overline{\mathbf{u}} \text{ and } \overline{\mathbf{v}} = 0. \tag{28}$$

Let $\mathbf{v} = (u, v, w)$; assuming a steady state and taking the dot product of $\mathbf{v}$ with equation (25) and integrating over the horizontal plane yields

$$-\overline{(uw)}\frac{dU}{dz} - \frac{g}{\rho_0}\overline{(\rho w)} - \overline{\epsilon} = 0. \tag{29}$$

Similarly, multiplying (26) by ρ and using the same procedure we get

$$\overline{(\rho w)}\frac{d\overline{\rho}}{dz} + \overline{\epsilon_\rho} = 0, \tag{30}$$

where $\overline{\epsilon}$ is the horizontally averaged momentum dissipation rate and $\overline{\epsilon_\rho}$ is the horizontally averaged thermal dissipation rate.

The following parameterizations were proposed by Townsend and follow from a simple dimensional analysis:

$$|\overline{uw}| = a_1 q^2, \quad |\overline{\rho w}| = a_2 r q, \quad \overline{\epsilon} = \frac{q^3}{L_\epsilon}, \quad \overline{\epsilon_\rho} = \frac{q r^2}{L_\rho} \tag{31}$$

where a_1, a_2 are positive nondimensional constants and L_ϵ, L_ρ are the (constant) integral length scales of velocity and density fluctuations. Substituting equation (30) into (26) to eliminate r yields a quadratic form for q only.

Townsend [25] then proceeded to use these equations to derive a relation between the local fluxes and the local Richardson number, defined in equation (2). However, we shall assume that the vertical variation of the flow and fluid structure is small, so that through a vertical integration of equations (29) and (25) we can obtain a relation between the global Richardson number J and the flux Richardson number R_f. The integration yields

$$\langle q\rangle_z^2 - \left(\frac{a_1 L_\epsilon \Delta U}{2d}\right)\langle q\rangle_z + \frac{g\Delta\rho L_\rho L_\epsilon a_2^2}{\rho_0 d} = 0, \tag{32}$$

where $\langle q\rangle_z$ results from the vertical integration of q, ΔU and $\Delta\rho$ are positive definite, and d is the half-thickness of the layer. This quadratic form can be solved for $\langle q\rangle_z$, and thereby provide also an expression for $\langle r\rangle_z$. These can then be substituted into the expression for the flux Richardson number, defined in (19) to give

$$R_f = \mathcal{E}_c = \frac{1}{2}\left(1 - \sqrt{1 - \frac{4\langle|\rho w|^2\rangle_z\langle\epsilon\rangle}{\langle|uw|^2\rangle_z\langle\epsilon_\rho\rangle_z}J}\right). \tag{33}$$

It appears that if J exceeds the critical value

$$\frac{\langle|uw|^2\rangle_z\langle\epsilon_\rho\rangle_z}{4\langle|\rho w|^2\rangle_z\langle\epsilon\rangle}, \tag{34}$$

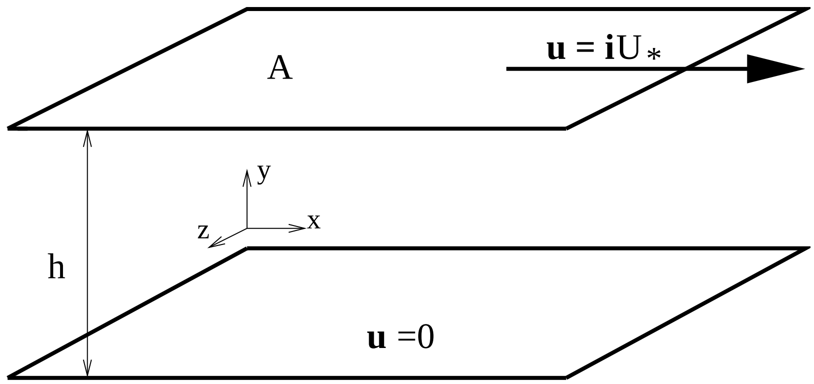

Figure 5: Schematic picture of set-up of numerical scheme

then there is no solution with physical meaning. As J tends to this critical value from below, $\mathcal{E}_c \to 1/2$. Townsend interprets the critical value as the point above which "the energy supply is no longer sufficient and the motion collapses to almost laminar flow".

Heuristically, this theory appears to suggest an upper bound on mixing efficiency of 1/2, consistently with the recent experimental and observational data.

We shall now try to apply the methods developed by Doering & Constantin [26] to a model flow in order to derive rigorous upper bounds for the irreversible mixing rate $\mathcal{M}$ or equivalently the long-time average of the buoyancy flux, motivated by these suggestions that R_f can be higher than is commonly assumed.

7 Bounding Techniques for Stratified Shear Flows

More specifically, for the problem of a stratified shear flow, the questions that we will ask are the following:

- Is it possible to generate a bound on mixing of heat?
- For a given forcing, how much energy is transferred into $\mathcal{P}$ the potential energy?
- Can we bound the long-time averaged buoyancy flux, i.e. can we bound the mixing rate $\mathcal{M}$? Does it depend on flow parameters? What is the associated mixing efficiency?

7.1 Model Problem by C. P. Caulfield and R. R. Kerswell [27]: Stratified Couette Flow

A simple model set-up that can be used for to investigate these issues is that of the stratified Couette Flow: two infinite bounding plates, placed at $z_{\pm} = \pm 1/2$, and moving with velocities $-\Delta U/2$ and $\Delta U/2$ respectively within our non-dimensional scheme. The temperature imposed on these plates is constant and fixed in such a way as to ensure $\rho = \rho_A \mp \Delta\rho/2$ on the upper and lower plates respectively. The set-up is illustrated in figure 5. It is important to stress that this flow is statically stable, as distinct from more commonly considered convectively unstable flows.

Using the following scales

- length: d,
- time: d^2/κ,
- density: $\Delta\rho$,

as well as the Boussinesq approximation, the governing equations (25)–(27) become

$$\begin{aligned}
\frac{D\mathbf{u}}{Dt} + \nabla p - \sigma\nabla^2\mathbf{u} + \sigma^2 Re^2 J\hat{\mathbf{z}} &= 0, \quad (\mathcal{NS}) && (35)\\
\frac{\partial\rho}{\partial t} + \mathbf{u}\cdot\nabla\rho - \nabla^2\rho &= 0, \quad (\mathcal{R}) && (36)\\
\nabla\cdot\mathbf{u} &= 0, && (37)
\end{aligned}$$

where the relevant parameters are

$$Re = \frac{\Delta U d}{\nu}, \qquad \sigma = \frac{\nu}{\kappa}, \qquad J = \frac{g\Delta\rho d}{\rho_0(\Delta U)^2}, \tag{38}$$

and the boundary conditions are

$$\begin{aligned}
\mathbf{u}(z_\pm) &= \mp\sigma Re\hat{\mathbf{x}}, && (39)\\
\rho(z_\pm) &= \mp 1/2. && (40)
\end{aligned}$$

7.2 Problem of Interest

We will be particularly interested in long-time averages of the flow in order to define bounds on the states reached by the system under forcing.

We perform the standard manipulation of dotting $\mathcal{NS}$ with $\mathbf{u}$; the long time average of the result yields the energy balance equation

$$\lim_{t\to\infty}\frac{1}{t}\int_0^t \langle|\nabla u|^2\rangle + \sigma Re^2 J\langle u_3\rho\rangle + \frac{\sigma Re}{2}\left[\left.\frac{\partial\bar{u}}{\partial z}\right|_{z_+} + \left.\frac{\partial\bar{u}}{\partial z}\right|_{z_-}\right] dt' = 0, \tag{41}$$

where here a bar denotes the horizontal average of a quantity and angle brackets denote the average over all three space dimensions. Similar manipulations of the mass continuity equation give an entropy equation

$$\lim_{t\to\infty}\frac{1}{t}\int_0^t \langle|\nabla\rho|^2\rangle + \frac{1}{2}\left[\left.\frac{\partial\bar{\rho}}{\partial z}\right|_{z_+} + \left.\frac{\partial\bar{\rho}}{\partial z}\right|_{z_-}\right] dt' = 0, \tag{42}$$

in the Boussinesq approximation, and finally multiplying the mass equation $\mathcal{R}$ by z and averaging yields the potential energy equation

$$\lim_{t\to\infty}\frac{1}{t}\int_0^t 1 + \langle u_3\rho\rangle + \frac{1}{2}\left[\left.\frac{\partial\bar{\rho}}{\partial z}\right|_{z_+} + \left.\frac{\partial\bar{\rho}}{\partial z}\right|_{z+-}\right] dt' = 0. \tag{43}$$

Eliminating the boundary terms between these two equations provides a relation between the long-term averaged buoyancy flux $\mathcal{B}$ and diffusion terms, and shows that maximizing

$$\mathcal{B} = \lim_{t\to\infty} \frac{1}{t} \int_0^t \sigma Re^2 J \langle u_3 \rho \rangle dt', \tag{44}$$

is equivalent to maximizing

$$\lim_{t\to\infty} \frac{1}{t} \int_0^t (\sigma Re^2 J \langle |\nabla\rho|^2 \rangle - 1) dt'. \tag{45}$$

Note that the quadratic form in $\nabla\rho$ is more convenient to maximize, which is why it was chosen. To consider this problem, we use the Constantin–Doering–Hopf Method [26], also called the "background method".

7.3 Constantin–Doering–Hopf Method

We decompose $\mathbf{u}$ and ρ in the following manner:

$$\mathbf{u}(\mathbf{x},t) = \phi(z)\hat{\mathbf{x}} + \mathbf{v}(\mathbf{x},t), \tag{46}$$

$$\rho(\mathbf{x},t) = \tau(z) + \theta(\mathbf{x},t). \tag{47}$$

Note that the background fields $\phi(z)$ and $\theta(z)$ are not the horizontal averages of the flow; this decomposition is certainly not unique, and allows us to chose the "background" fields $\phi(z)$ and $\theta(z)$ arbitrarily under the sole conditions that they satisfy the inhomogeneous boundary conditions with the fluctuations $\mathbf{v}$ and θ satisifying the homogeneous boundary conditions, i.e. $\phi = \mp\sigma Re$, $\tau = \mp 1/2$, $\mathbf{v} = \mathbf{0}$, and $\theta = 0$ at $z_\pm$.

The corresponding variational problem consists in maximizing the functional

$$\mathcal{L}(\phi,\tau,a,b,\mathbf{v},\theta) = \lim_{t\to\infty} \frac{1}{t} \int_0^t \left[\sigma Re^2 J \left\langle \left| \frac{\mathrm{d}\tau}{\mathrm{d}z}\hat{\mathbf{z}} + \nabla\theta \right|^2 \right\rangle - a\langle \mathbf{v}\cdot(\mathcal{NS})\rangle - b\langle\theta(\mathcal{R})\rangle \right] dt', \tag{48}$$

and where, formally $a\mathbf{v}$ is the Lagrange multiplier used to impose the condition that the flow should satisfy the Navier Stokes equation, and $b\theta$ is the Lagrange Multiplier used to impose ($\mathcal{R}$). This is actually equivalent to the statement that $-a\phi$ is the multiplier used to impose the mean momentum balance, a is the multiplier used to impose the total power balance, b the entropy flux balance and finally $-b\tau$ the mean heat balance, which can be shown from (48).

7.4 Spectral Constraint

Substituting the ansatz (47) into the expressions for ($\mathcal{NS}$) and ($\mathcal{R}$) of the functional $\mathcal{L}$ yields

$$\mathcal{L} = \sigma Re^2 J \langle {\tau'}^2 \rangle - \lim_{t\to\infty} \frac{1}{t} \int_0^t \mathcal{G}(\tau,\phi,\mathbf{v},\theta) dt', \tag{49}$$

where the prime denotes derivative with respect to z. Provided the infimum of $\mathcal{G}$ exists, then

$$\mathcal{L} \leq \sigma Re^2 J\langle {\tau'}^2\rangle - \inf_{\mathbf{v},\theta} \mathcal{G}, \tag{50}$$

where

$$\begin{aligned} \mathcal{G} \quad = \quad & \langle a\sigma|\nabla v|^2 + (b - \sigma Re^2 J)|\nabla\theta|^2 + av_1 v_3\phi' \\ & + (b\tau' + a\sigma^2 Re^2 J)v_3\theta - (b - 2\sigma Re^2 J)\theta\tau'' - a\sigma\phi'' v_1\rangle. \end{aligned} \tag{51}$$

Convexity arguments show that the infimum exists only if:

$$\langle a\sigma|\nabla v|^2 + (b - \sigma Re^2 J)|\nabla\theta|^2 \quad + av_1 v_3\phi' + (b\tau' + a\sigma^2 Re^2 J)v_3\theta\rangle \geq 0, \ \{\mathcal{SC}\} \tag{52}$$

which represents the so-called spectral constraint. This implies straightforwardly that a and b must necessarily satisfy $a\sigma > 0$ and $b > \sigma Re^2 J$.

The Euler–Lagrange equations which must be satisfied to minimize $\mathcal{G}$ are given by

$$\begin{aligned} \frac{\delta\mathcal{G}}{\delta\mathbf{v}} = -2a\nabla^2\mathbf{v} + a\phi' + (b\tau' + a\sigma^2\mathrm{Re}^2 J)\theta\hat{\mathbf{z}} + \nabla p - a\sigma\phi''\hat{\mathbf{x}} \quad &= \quad 0, \\ \frac{\delta\mathcal{G}}{\delta\theta} = -2(b - \sigma\mathrm{Re}^2 J)\nabla^2\theta + (b\tau' + a\sigma^2\mathrm{Re}^2 J)v_3 - (b - 2\sigma\mathrm{Re}^2 J)\tau'' \quad &= \quad 0. \end{aligned} \tag{53}$$

From these, the horizontally averaged part of these equations can be solved straightforwardly to provide the extremal mean parts:

$$\overline{v}^\star \quad = \quad -\frac{1}{2}(\phi + \sigma Rez)\hat{\mathbf{x}}, \tag{54}$$

$$\overline{\theta}^\star \quad = \quad \frac{(2\sigma Re^2 J - b)}{2(b - \sigma Re^2 J)}(\tau + z), \tag{55}$$

where the background fields ϕ and τ are subject to the spectral constraint $\mathcal{SC}$. For these extremalising fields, the functional $\mathcal{F}$ has a conservative upper bound of

$$\mathcal{L} \leq \mathcal{L}_{\max} = \frac{b^2}{4(b - \sigma Re^2 J)}\langle(\tau' + 1)^2\rangle + \sigma Re^2 J + \frac{\sigma}{4}\langle(\phi' + \sigma Re)^2\rangle. \tag{56}$$

7.5 Distilled Variational Problem

The remainder of the problem now consists in chosing the background fields τ and ϕ that satisfy the boundary conditions as well as the spectral constraints in order to make $\mathcal{L}_{\max}$ as small as possible. However, instead of optimizing the problem by spanning through all τ and ϕ possible, we will limit the study to a specific family of functions (with a boundary layer structure suggested by physical intuition) and minimize $\mathcal{L}_{\max}$ within that family. This restricted class of functions will undoubtedly lead us to an upper bound, but at this stage there is no way of knowing how conservative this bound will prove to be.

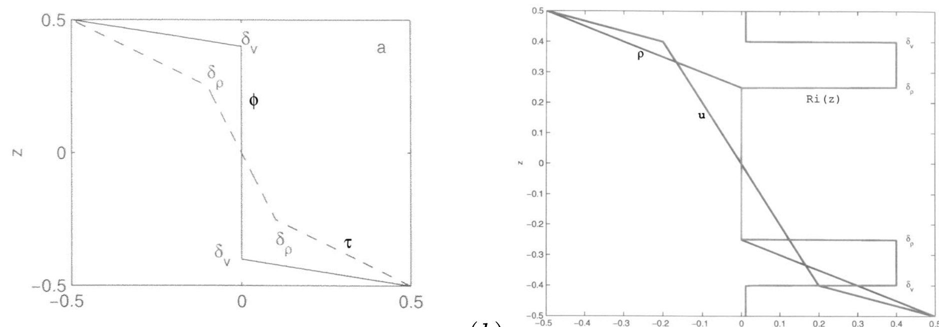

(a) (b)

Figure 6: Form of the extremalizing solutions: (a) shows ϕ (solid) and τ (dashed) and (b) shows the $\mathbf{u}$ and ρ for the same case with the Richardson number also shown.

The functions ϕ' and τ' are chosen to have a piece-wise linear structure with:

$$\phi'(z) = \begin{cases} -\frac{\sigma Re}{2\delta_v} & \text{upper } \delta_v, \\ 0 & \text{interior}, \\ -\frac{\sigma Re}{2\delta_v} & \text{lower } \delta_v, \end{cases}$$

$$\tau'(z) = \begin{cases} -\left(\frac{b - a\sigma^2 Re^2 J(1-2\delta_\rho)}{2b\delta_\rho}\right) & \text{upper } \delta_\rho, \\ -\frac{a\sigma^2 Re^2 J}{b} & \text{interior}, \\ -\left(\frac{b - a\sigma^2 Re^2 J(1-2\delta_\rho)}{2b\delta_\rho}\right) & \text{lower } \delta_\rho. \end{cases}$$

The graphs of the extremalizing solution are shown in figure 6.

Substituting the extremalising fields into equation (47), and combining these with the ansatz for τ and ϕ into the energy, entropy and potential energy conservation equations (41,42,43) yields a unique relation between the Lagrange multipliers a and b as well as conditions on the thicknesses of the boundary layers δ_ρ and δ_v:

$$b = (2 - a\sigma)\sigma Re^2 J, \tag{57}$$

$$\frac{1 - 2\delta_v}{2\delta v} = \frac{4J}{\sigma}\left[\frac{1 - 2\delta_\rho}{2\delta_\rho}\right], \tag{58}$$

with $0 < a\sigma < 1$. Therefore

$$\mathcal{L}_{\max} = \frac{\sigma Re^2 J}{2\delta_\rho} = \frac{\sigma^2 Re^2}{4}\left[\frac{1 - 2\delta_v}{2\delta_v} + \frac{4J}{\sigma}\right], \tag{59}$$

still subject to the spectral constraints $\mathcal{SC}$.

7.6 Simplified Spectral Constraint

We shall again simplify the spectral constraints by using a conservative estimate, effectively separating the effects of velocity and density variation and requiring each to be satisfied independently. Using functional analysis together with the Cauchy–Schwartz inequality, it can be proven that the spectral constraints are satisfied provided that

$$a\sigma - \frac{a\sigma Re\delta_v}{8\sqrt{2}} - \frac{\sigma Re^2 J^3 \delta_v^2 (1-a\sigma)}{(\sigma - 2\delta_v[\sigma - 4J])^2} \geq 0. \tag{60}$$

In order to find a rigorous upper bound we must therefore minimize $\mathcal{L}_{\max}$ subject to the conditions (60) and $0 < a\sigma < 1$. Additional manipulations show that $\mathcal{L}_{\max}$ is minimized when δ_v is maximized and for $Re > 16\sqrt{2} = 22.6$ it attains the minimal value when

$$\delta_v = \delta_v^\star = \frac{8\sqrt{2}}{Re}. \tag{61}$$

It follows that

$$\begin{aligned}
\delta_\rho^\star &= \frac{32\sqrt{2}J}{\sigma(Re - 16\sqrt{2}) + 64\sqrt{2}J}, && (62)\\
a^\star\sigma &= 1, && (63)\\
b^\star &= \sigma Re^2 J, && (64)\\
\mathcal{L}_{\max} &= \frac{\sigma^2 Re^3}{64\sqrt{2}}\left(1 - \frac{16\sqrt{2}}{Re}\right) + \sigma Re^2 J, && (65)\\
\mathcal{B} &\leq \mathcal{B}_{\max} = \frac{\sigma^2 Re^3}{64\sqrt{2}}\left(1 - \frac{16\sqrt{2}}{Re}\right). && (66)
\end{aligned}$$

8 Implications

Certain characteristics of the bounding flow are worthy of note. The total dissipation rate is given by

$$\langle |\nabla u^\star|^2 \rangle = \frac{\sigma^2 Re^2}{4}\left(\frac{Re}{16\sqrt{2}} + 3\right), \tag{67}$$

which is, perhaps surprisingly, independent of the bulk Richardson number J. However, we shall see that this result is consistent with the initial assumptions on the flow. The dimensional dissipation rate ϵ is given by

$$\epsilon = \frac{U^3}{64\sqrt{2}d}, \tag{68}$$

which has exactly the same scaling as that in the homogeneous Couette case. Again this result suggests that the flow stratification seems to have little influence on the global features of mixing in this problem, consistently with the underlying assumptions of Weinstock and Townsend. Similarly, it is found that both the long-time averaged buoyancy flux $\mathcal{B}_{\max}$ & and the long-time averaged flux Richardson number (or equivalently the cumulative mixing efficiency $\mathcal{E}_c$) are independent of J, where

$$\mathcal{E}_c = \frac{\mathcal{B}}{\mathcal{B} + \langle |\nabla u|^2 \rangle} = \frac{1 - \sigma^2 Re^2/\langle |\nabla u|^2 \rangle}{2 - \sigma^2 Re^2/\langle |\nabla u|^2 \rangle}. \tag{69}$$

When the Reynolds number Re tends to infinity, $\mathcal{E}_c$ tends to the limit 1/2 which suggests an equipartition of the total energy intput into the fluid between the viscous dissipation and the buoyancy flux (i.e. the irreversible changes to the potential energy) consistently with both recent observatons of Fernando and co-workers and the heuristic theoretical considerations of Weinstock and Townsend. The velocity boundary layer thickness is independant of the stratification and scales like $1/Re$ as Re increases.

However, the overall stratification still has an important role in the determination of the thickness of the density boundary, for example, or in the local gradient Richardson number Ri; near the walls, it is indeed defined as

$$Ri^{\dagger}(\pm 1/2) = \frac{16\sqrt{2}\left[\sigma\left(Re - 16\sqrt{2}\right) + 4J\right]}{(Re + 16\sqrt{2})^2}, \tag{70}$$

$$\simeq \frac{16\sqrt{2}\sigma}{Re}. \tag{71}$$

However, we see here again that $Ri \to 16\sqrt{2}\sigma/Re$ as $Re \to \infty$, suggesting that as the forcing is increased, the stratification is irrelevant to the flow in the boundary layers near the wall.

The interpretation of the results is that in the long-term averaged bounding flow, the middle layer is well-mixed and the mixing occurs principally in the boundary layers. In these thin layers the stratification does not dominate and the turbulence is driven through the shear on the walls; its characteristics depend principally on Re and not on Ri. We also note that the optimal shear in the bulk of the flow doesn't vanish completely, and is reduced by 50% from the laminar solution. This result is compatible with numerical experiments and observations, althoung not with the observed behaviour of usntratified Couette flows.

9 Conclusions and Future Directions

We have seen that mixing in stratified shear flows is an important problem. However, there is a wide variability in the estimates of mixing found so far, although the evidence suggests that the efficiency of mixing is a good way to describe the process.

Initial work with Bounding methods suggest that they can contribute greatly to our understanding of the problem, but there are still many open problems. For example, we would like to achieve a bound on mixing and to compare the conservative estimates of the flow with the actual flows obtained. Also we need to relate $\mathcal{E}_c$ to instantaneous values of R_f and in particular develop rigorous bounds of both $\mathcal{E}_c$ and R_f. We also at the moment have no way of knowing how widely the results of bounding studies on highly simplified model problems can be applied to typical geophysical flows or indeed, whether our results can be embedded in an improved parameterization. There is clearly much more work to be done on this important problem.

References

[1] K. B. Winters, P. N. Lombard, J. J. Riley, and E. A. D'Asaro, "Available potential energy and mixing in density-stratified fluids," J. Fluid Mech. **289**, 115 (1995).

[2] Y. G. Park, J. A. Whitehead, and A. Gnanadeskian, “Turbulent mixing in stratified fluids – layer formation and energetics,” J. Fluid Mech. **279**, 279 (1994).

[3] L. H. Shih, J. R. Koseff, J. H. Ferziger, and C. R. Rehmann, “Scaling acid parameterization of stratified homogeneous turbulent shear flow,” J. Fluid Mech. **412**, 1 (2000).

[4] K. B. Winters and E. A. D’Asaro, “Diascalar flux and the rate of fluid mixing,” J. Fluid Mech. **317**, 179 (1996).

[5] T. R. Osborn, “Estimates of the local rate of vertical diffusion from dissipation measurements,” J. Phys. Ocean. **10**, 83 (1980).

[6] M. C. Gregg, “Diapycnal mixing in the thermocline - A Review,” J. Geophys. Res. – Oceans **92(c5)**, 5249 (1987).

[7] N. S. Oakey, “Determination of the rate of dissipation of turbulent energy from simultaneous temperature and velocity shear microstructure measurements,” J. Phys. Ocean. **12**, 256 (1982).

[8] H. J. S. Fernando, “Turbulent mixing in stratified fluids,” Ann. Rev. Fluid Mech. **23**, 35 (1991).

[9] O. M. Phillips, “Turbulence in a strongly stratified fluid – is it unstable?,” Deep-Sea Res. **19**, 79 (1972).

[10] E. S. Posmentier, “The generation of salinity fine structures by vertical diffusion,” J. Phys. Ocean. **7**, 298 (1977).

[11] J. H. Lienhard and C. W. Vanatta, “The decay of turbulence in thermally stratified flow,” J. Fluid Mech. **210**, 57 (1990).

[12] G. N. Ivey and J. Imberger, “On the nature of turbulence in a stratified fluid. Part I: The energetics of mixing,” J. Phys. Ocean. **21**, 650 (1990).

[13] A. A. Townsend, “The effects of radiative transfer on turbulent flow of a stratified fluid,” J. Fluid Mech. **3**, 361 (1958).

[14] G. L. Mellor and T. Yamada, “Development of a turbulence closure model for geophysical fluid problems,” Rev. of Geophys. Space Phys. **20**, 851 (1982).

[15] M. Nakanishi, “Improvement of the mellor–yamada turbulence closure model based on large eddy simulation data,” Bound.-Layer Met. **99**, 349 (2001).

[16] E. R. Pardyjak, P. Monti, and H. J. S. Fernando, “Flux richardson number measurements in stable atmospheric shear flows,” J. Fluid Mech. **459**, 307 (2002).

[17] E. J. Strang and H. J. S. Fernando, “Vertical mixing and transports through a stratified shear layer,” J. Phys. Ocean. **31**, 2026 (2001).

[18] C. P. Caulfield and W. R. Peltier, “The anatomy of the mixing transition in homogeneous and stratified shear layers,” J. Fluid Mech. **413**, 1 (2000).

[19] W. D. Smyth and J. N. Moum, "Length scales of turbulence in stably stratified mixing layers," Phys. Fluids **12**, 1327 (2000).

[20] W. D. Smyth and J. N. Moum, "Anisotropy of turbulence in stably stratified mixing layers," Phys. Fluids **12**, 1343 (2000).

[21] Rottman and Stretch, (2002).

[22] W. J. Heck and H. A. Panofsky, "Stratospheric mixing estimates from heat flux measurements," The Natural Stratosphere of 1974, CIAP Monogr. **No. 2, Dept. of Transportation TST-75-51**, 6 (1975).

[23] H. J. Pearson, J. S. Puttock, and J. C. R. Hunt, "A statistical-model of fluid-element motions and vertical diffusion in a homogeneous stratified turbulent-flow," J. Fluid Mech. **129**, 219 (1983).

[24] J. Weinstock, "Vertical turbulent diffusion in a stably stratified fluid," J. Atmos. Sci. **35**, 1022 (1978).

[25] A. A. Townsend, *The Structure of Turbulent Shear Flow*, 2 ed. (Cambridge University Press, Cambridge, 1976).

[26] C. R. Doering and P. Constantin, "Energy-dissipation in shear driven turbulence," Phys. Rev. Lett. **69**, 1648 (1992).

[27] C. P. Caulfield and R. R. Kerswell, "Maximal mixing rate in turbulent stably stratified Couette flow," Phys. Fluids **13**, 894 (2001).